International Journal of Manufacturing Economics and Management
ISSN 2784-1278 ISSN-L 2784-1278, Vol. V, No. 2 / 2025
https://doi.org/10.54684/ijmem.2025.5.2.53

HYBRID POLYMER STRUCTURE - INTERFACIAL ADHESION AND MECHANICAL BEHAVIOUR OF INJECTION-MOLDED/FFF PART

Simona-Nicoleta Mazurchevici

"Gheorghe Asachi" Technical University of Iasi, Department of Machine Manufacturing Technology, Blvd. Mangeron, No. 59A, 700050, Iasi, Romania

Corresponding author: Simona-Nicoleta Mazurchevici, simona-nicoleta.mazurchevici@academic.tuiasi.ro

Abstract: The growing demand for mass customization in Industry 4.0 drives the development of hybrid manufacturing strategies capable of combining the geometric flexibility of Fused Filament Fabrication (FFF) with the productivity of injection molding. This study investigates the mechanical behaviour and interfacial adhesion of hybrid tensile specimens produced by overmolding Arboblend V2 Nature onto 3D-printed PLA reinforcement structures. Tensile testing revealed a brittle response, with an average strength of 8.92 MPa and an elastic modulus of 1039 MPa, significantly lower than monolithic Arboblend or PLA, primarily due to interfacial debonding, anisotropy, and porosity inherent in FFF structures. SEM and optical microscopy confirmed limited polymer chain diffusion at the interface, incomplete bonding, and microvoids characteristic of layered deposition. Injection molding simulations showed efficient cavity filling, acceptable thermal gradients, and low warpage, supporting the manufacturability of the hybrid design. The findings demonstrate that interface temperature, material drying, and geometric optimization of the reinforcement structure are key factors for improving adhesion and overall performance. This hybrid approach provides a viable pathway toward medium-volume personalized polymer components, enabling tailored mechanical properties through controlled design of embedded 3D-printed structures.

1. INTRODUCTION

The mass customisation of production to satisfy each customer's unique wants is the current industrial trend that is in line with Industry 4.0 standards. When several conventional manufacturing processes are integrated into the creation of a single component, this kind of synergy can be attained. The combination of injection molding with additive manufacturing (AM) is one of the most promising. AM provides significantly greater design freedom compared to traditional manufacturing, enabling even highly sophisticated geometries to be produced at a reasonable cost. However, a key limitation of AM is the production rate, which is several orders of magnitude slower than conventional high-volume polymer processing technologies. Conversely, injection molding is a large-scale manufacturing technique with limited customization capabilities, and adapting injected parts to new geometries is often costly and time-consuming.

The modern plastics industry is currently undergoing significant changes driven by market demands. One prominent trend is mass individualization, which requires increasing product and process diversity while maintaining high-volume production, [1]. Injection molding remains the most efficient and established technology for mass production, yet it is often associated with high tooling costs, long mold development times, and limited flexibility when design modifications are required. In contrast, AM—although relatively new compared to injection molding—generally involves lower initial costs and is regarded as a highly versatile process, [2, 3].

AM enables the creation of complex structures that are typically difficult or even impossible to produce by traditional methods. For instance, AM can fabricate optimized structures, [4] and can significantly simplify the transfer of laboratory-scale results into industrial products, [5]. However, the slow manufacturing rate—typically three to four orders of magnitude lower than injection molding—remains its principal disadvantage [6]. Hybrid methods, which integrate many polymer processing processes to produce a single part, can strike a balance between high production speed and product customisation [7–10].

Combining AM with injection molding can greatly enhance product versatility, though often at the expense of production speed. In applications requiring complex geometries paired with high load-bearing capacity, traditional manufacturing routes become economically impractical. Consequently, original equipment manufacturers (OEMs) increasingly rely on hybrid technologies to produce polymer and polymer-based

composite components. For example, TxV Aero Composites recently manufactured an aircraft overhead luggage bin support structure using a hybrid technology involving overmolding, [11].
Areas where AM combined with injection molding is economically feasible are most likely medium-scale production environments. Literature analysis shows that this combination is particularly suitable for medium-volume manufacturing requiring high customization levels. For example, Laptoiu et al. [12] suggested using a hybrid AM–injection molding technique to create customized bi-material hand orthoses. While the soft portion of the orthosis was injected using a fast-curing silicone, the rigid portion was 3D printed from PLA. Interestingly, the authors referred to their process as injection molding, although it was likely a reactive injection process. Kim et al. [13], proposed combining automated tape placement of long glass-fiber reinforced polypropylene with injection molding of short-fiber reinforced polypropylene to manufacture an automotive bumper component. Brecher et al. [14], produced a hybrid composite truss structure by combining a carbon-fiber sheet material with a 3D-printed PA12 stiffening architecture.
The ability to combine AM with injection molding has led to a variety of manufacturing concepts. For example, a rigid substrate may be produced by injection molding first, after which additional features can be added by AM, or the process may occur in reverse order, [15]. Another interesting concept uses AM to fabricate 3D preforms that serve as reinforcement structures within a composite. Since AM builds parts layer by layer, even highly complex 3D parts can be manufactured.
Three different orthogonal 3D preforms made of ABS reinforced with short carbon fibers were created by Chou et al. [16]. These preforms were then impregnated with an elastomeric system based on silicone. The authors stressed the necessity of scaling up AM to reach industrial production rates, even if they showed the concept's viability. In 2017, Markforged patented a similar approach in which the preform is made from continuous carbon fibers and subsequently overmolded with a thermoplastic matrix, [15].
Kazmer and Colon proposed "injection printing," another hybrid concept [17]. This method entails creating a 3D-printed shell and injecting molten polymer into it. When compared to traditional 3D printing, the average improvement in manufacturing speed using this technology was 3.2.
Rapid tooling (RT) for injection molding is another intriguing hybrid idea. Injection molds may be produced in a matter of days or even hours at a reasonable cost, thanks to RT [18, 19], which significantly shortens time-to-market and allows manufacturing systems to quickly adjust to evolving product designs.
The adhesion between components, which is usually far weaker than the strength of a monolithic part, is AM's primary limitation, even though combining AM with injection molding is promising for medium-scale tailored production of polymers and composites.
Numerous studies have investigated improving bonding strength through optimization of process parameters, [20–23], surface treatments, [37], or by creating mechanical interlocking between bonded components, [12, 24–26]. Nevertheless, the majority of these studies do not examine hybrid technologies and instead focus on bonding problems within a single manufacturing process.
When chemical bonding is inadequate or may deteriorate over time, mechanical interlocking is very useful. There are various methods to enhance mechanical adhesion between two components. For instance, Laptoiu et al. [12] showed how well cylindrical interlocking points work to connect an overmolded silicone component to an additively created substrate. Another method is to make infill patterns in the base plate along the contact zone. The molten polymer fills these patterns during overmolding, creating micro-mechanical interlocking at the interface. Literature suggests that modifying FFF parameters influences the tensile properties and quality of printed parts. However, only a limited number of studies have investigated the bonding strength between printed and injection-molded components. Therefore, the objective of this work is to investigate the adhesion between additively manufactured and injection-molded components.
In the present study, a solution for mass customization was proposed: a 3D-printed sample acting as a reinforcement, followed by injection overmolding of a rigidizing element. The adhesion between the 3D-printed component and the injected polymer was analyzed in detail. The study also includes a simulation of mold filling while the printed samples are positioned in the active side of the mold. Arboblend V2 Nature was used as the injected material, while PLA (green) was used for printing.

2. MATERIALS AND METHODS

For the fabrication of the reinforcement samples, a Bambu Lab X1-Carbon printer was used, operating with the Fused Filament Fabrication (FFF) method. The filament diameter was 1.75 mm, and the printing material was polylactic acid (PLA). G-code generation was performed using Bambu Studio software, version 2.1.1.52. The printing parameters were as follows: layer height 0.08 mm; first layer (support) height 0.2 mm; nozzle diameter

0.4 mm; infill pattern: grid; infill density: 90%; extruder temperature: 220 °C; bed temperature: 55 °C; and infill speed: 150 mm/s.
The injection molding process was carried out using an SZ800H injection molding machine, belonging to the category of horizontal machines with a single injection cylinder. Arboblend V2 Nature granules were injected according to DIN EN ISO 527-1:1993. The active plate of the mold was set at an injection angle of 0°. The processing parameters were: injection temperature – 168 °C, injection direction – 0°, injection pressure – 80 MPa, injection time – 31 s, cooling time – 20 s, and screw displacement/injection speed – 60 m/min.
Figure 1(b) presents the injection-molded samples, whereas Figure 1(a) shows the positioning of the 3D-printed reinforcement structures inside the cavities of the active plate.
The tensile samples were produced by conventional injection molding using Arboblend V2 Nature, while the reinforcement structure was manufactured by FFF 3D printing from biodegradable PLA. Black PLA was used during process optimization and parameter adjustment, and green PLA was used for the samples intended for mechanical testing.

(a) (b)

Fig. 1. Obtaining the reinforced samples: (a) positioning of the reinforcement structure inside the cavities of the active mold plate; (b) injection-molded samples reinforced with the 3D-printed structure

For the tensile testing of the samples, a standardized Instron 3382 universal testing machine was used, capable of applying loads of up to 100 kN.
Scanning Electron Microscopy (SEM) analysis was performed using a QUANTA 200 3D scanning electron microscope. Micrographic maps were acquired both in the complete fracture region of the sample following tensile loading and along the longitudinal section of the specimen.
Additionally, in order to enhance the visual differentiation (color contrast) between the printed and injection-molded regions, a Leica CTR4000 optical microscope was employed.

3. SIMULATION OF THE INJECTION MOLDING PROCESS FOR POLYMER-REINFORCED PROTOTYPE STRUCTURES

3.1 Modeling of the Printed/Injected Samples

SolidWorks modeling and simulation software was utilized to create the 3D models needed for the mechanical and injection molding simulations. The standard dog-bone configuration of the tensile sample model for polymer testing (Figure 2(a)) was developed in compliance with the applicable international standards. Furthermore, as seen in Figure 2(b), a different model designed to act as the reinforcing structure was created.
The physical tensile sample was produced using conventional injection molding with Arboblend V2 Nature as the molding material. The corresponding reinforcement structure was manufactured by Fused Filament Fabrication (FFF) using biodegradable PLA—black PLA for process tuning and parameter adjustment, and green PLA for the samples subjected to mechanical testing.
To simulate the filling behavior of the tensile part during injection molding, it was necessary to remove the reinforcement structure from the standard sample model, as illustrated in Figure 2(c), while accounting for the reinforcement geometry. The final reinforced sample configuration used in the simulation is presented in Figure 2(d).

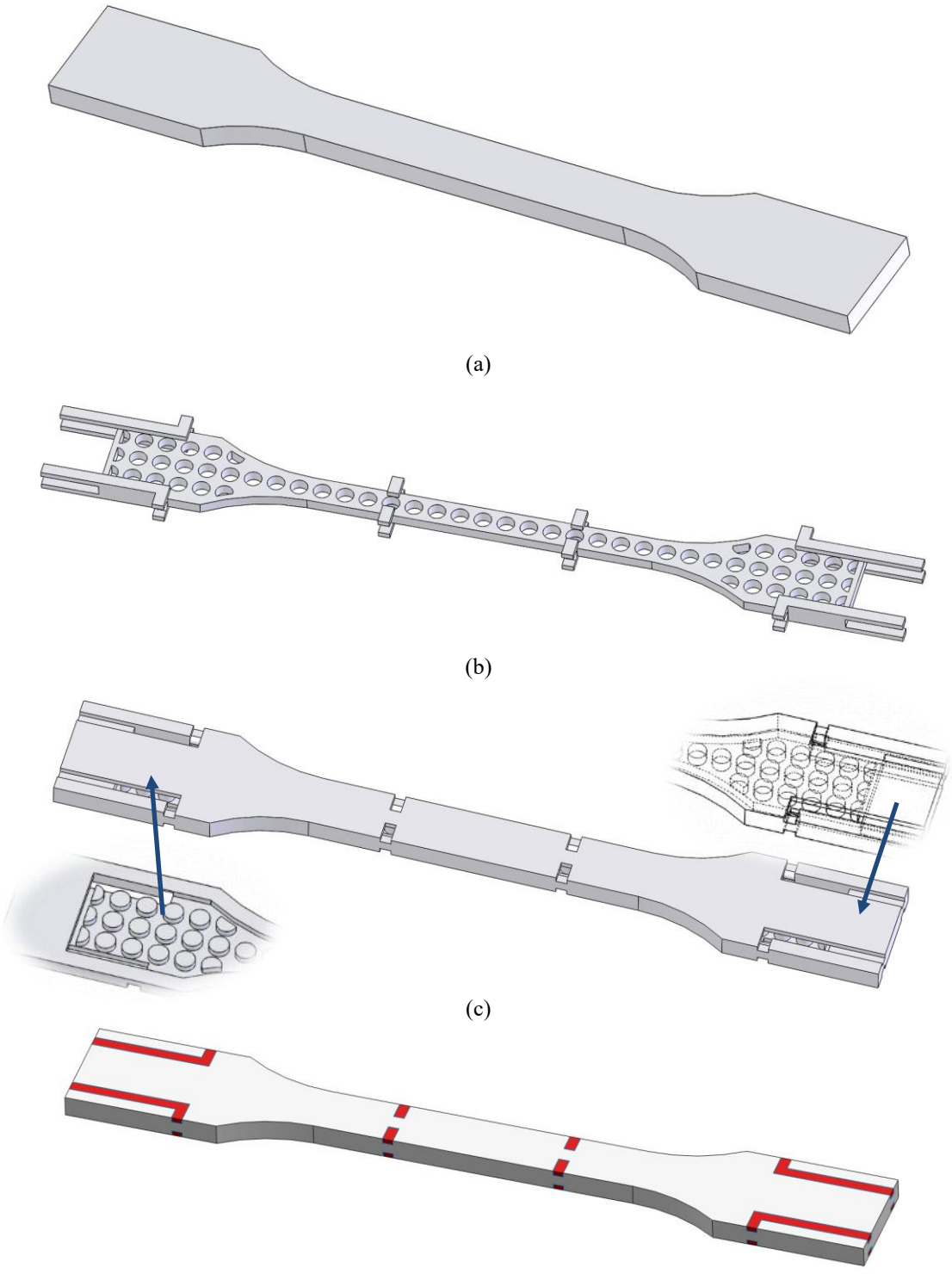

Fig. 2. 3D models: (a) tensile sample; (b) reinforcement structure for the tensile sample; (c) tensile sample without the reinforcement structure volume; (d) reinforced tensile sample.

The dimensions and geometry of the reinforcement structure, shown in Figure 2(b) and Figure 3, were selected to meet the following criteria:
- to enhance the mechanical performance of the samples;
- to allow proper centering within the cavity of the active mold plate;
- to ensure a central placement of the structure, with symmetrical support features that do not influence the mechanical testing results;
- to enable rapid filling of the remaining free volume during injection molding;
- to maximize the contact surface between the printed and injection-molded components in order to improve interfacial adhesion;

- to incorporate voids in the model that help reduce stresses arising during prototyping and injection molding.

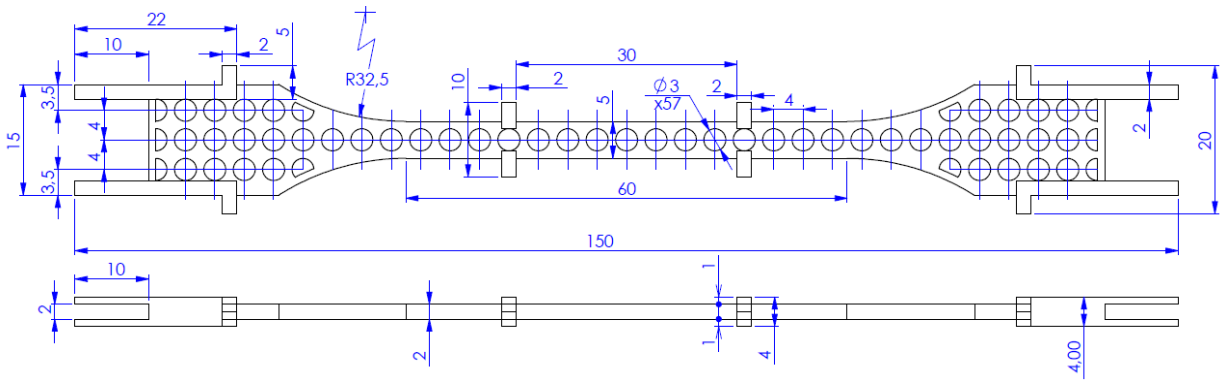

Fig. 3. Dimensions of the reinforcement structure

3.2 Simulation of the injection molding process

To analyze the behavior of the "injected sample with voids" during the injection molding process, a simulation was performed using the SolidWorks Plastics analysis module. The model used was a solid mesh consisting of 141,126 elements and 48,661 nodes, with a total volume of 6.76 cm³ and a mass of 8.78 g. The main dimensions of the part were 150 mm × 4 mm × 20 mm.

The material selected for the simulation was Arboblend V2 Nature, with a melting temperature of 167 °C and a mold temperature of 50 °C. Additional key material properties included a glass transition temperature of 60 °C, a Young's modulus of 2000 MPa, and a Poisson's ratio of 0.35.

The injection molding process was configured with a filling time of 0.8 seconds (Figure 5), a maximum injection pressure of 110 MPa, and a maximum clamping force of 100 tons. The holding pressure phase lasted 3.2 seconds, and the total packing stage time was 12.03 seconds, followed by a cooling time of 8.7 seconds, resulting in a complete molding cycle of 17.9 seconds.

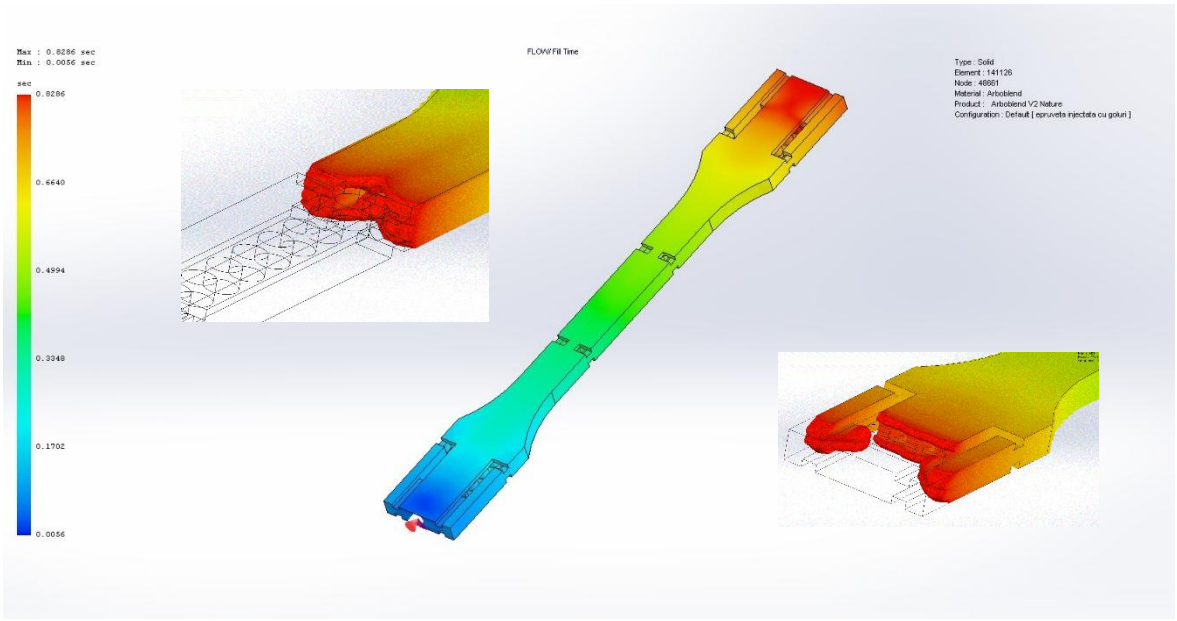

Fig. 4. Filling time of the sample

The results showed that the required injection pressure was 63.9 MPa, while the maximum melt temperature reached 171.3 °C (Figure 4). The maximum shear rate was 1703.9 s^{-1}, and the maximum shear stress was 0.68 MPa. During the packing stage, the maximum temperature decreased to 152.8 °C, and the volumetric shrinkage values were negligible.

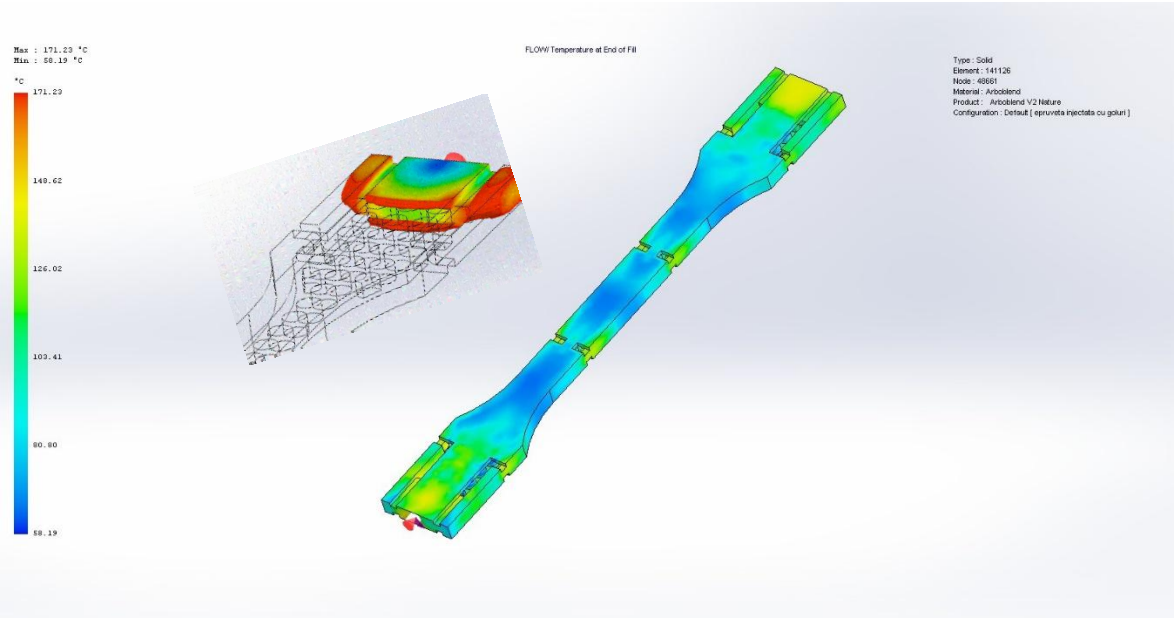

Fig.5. Maximum melt temperature

The warpage analysis indicated a maximum displacement of 0.1769 mm, with the largest deformation occurring along the X-direction (0.3494 mm), while significantly smaller values were observed along the Y and Z directions (0.0307 mm and 0.0818 mm, respectively). These results demonstrate that the part exhibits good dimensional stability, with minimal deformation after the cooling stage.

The total computation time for the simulation was 23.898 seconds, confirming both the complexity of the analysis and the high precision of the generated results. The obtained data provide valuable insights for optimizing the injection parameters so that the part can be manufactured with minimal defects and enhanced dimensional accuracy.

In conclusion, the simulation results show that the analyzed part demonstrates favorable behavior during the injection molding process, with low deformation levels and good dimensional stability. The selected processing parameters allow the sample to be fabricated without major defects and with an optimized cycle time. The total computation time of 23.898 seconds further confirms the complexity and accuracy of the applied simulation model.

4. RESULTS AND DISCUSSIONS

4.1 Tensile testing

Tensile testing of the samples (dimensionally compliant with ISO 527-2), injection-molded from Arboblend V2 Nature and reinforced with a PLA printed structure, revealed the brittle behavior of the composite material, as shown in Figure 6.

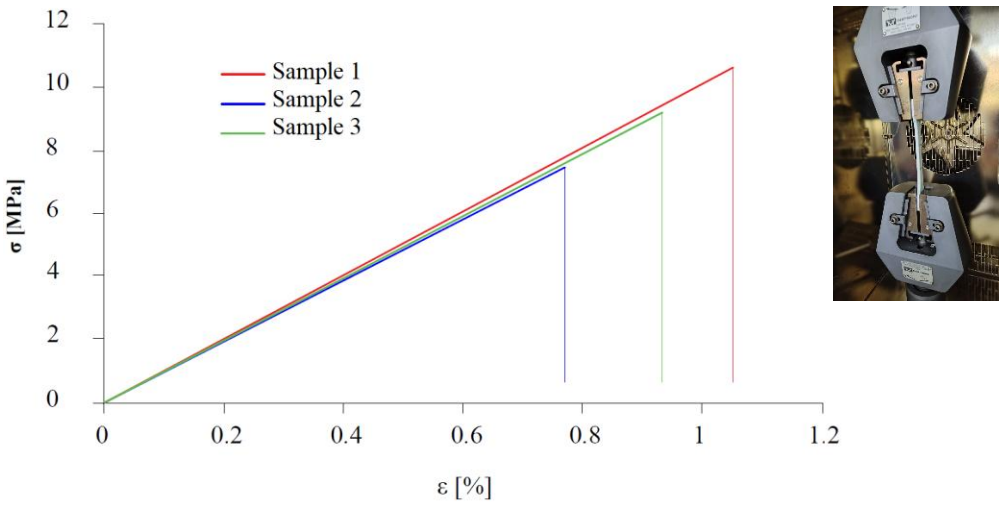

Fig.6. Stress–strain curve for the Arboblend + printed PLA sample

Tabelul 1. Experimental results of uniaxial tensile tests on injection-molded Arboblend V2 Nature samples reinforced with a PLA printed structure

Sample	σ_{max} [MPa]	ε [%]	E [MPa]
1	10.09	1.04	1088.97
2	7.39	0.76	992.08
3	9.28	0.93	1037.19
Average	**8.92±1.38**	**0.91±0.14**	**1039.41±48.48**

Analyzing the dispersion of the results for the three tested samples, it can be concluded that the composite material exhibits a low variability of the measured properties. According to the obtained values for the elongation at break (ε), the samples demonstrated a rigid behavior of approximately (1 ± 0.14)%, as shown in Table 1.

The reduction in the mechanical characteristics of the composite sample compared with a fully injection-molded Arboblend V2 Nature sample (σ_max ≈ 44 MPa, [27]) or with a fully 3D-printed PLA sample (≈ 51 MPa, [28]) can be attributed to several factors widely documented in the literature:

– *Anisotropy and porosity in the printed part (PLA reinforcement)*: Printed components inherently contain porosity both within individual deposited layers and between successive layers, even when a 90% infill density is used. The printing orientation, infill type and density, layer height, extrusion temperature, and other parameters significantly influence mechanical properties. Such voids and "cold joints" act as crack initiators and drastically decrease the tensile strength relative to injection-molded Arboblend or 3D-printed PLA. Reported tensile strengths for PLA vary widely (≈12–55 MPa), depending on the process parameters, and unfavorable orientations may yield values as low as 10–20 MPa, [29–31]. In this study, the sample was printed in a flat orientation on the build plate.

– *Poor adhesion during overmolding (PLA substrate/core - Arboblend overmold)*: The performance of an overmolded component depends strongly on interfacial contact and the diffusion of polymer chains at the interface. If the polymers are partially incompatible, the interface temperature is insufficient, contamination is present, or the contact time/temperature is too low, the interface remains weak and premature delamination occurs, which significantly reduces the mechanical performance of the composite—even when each material exhibits much higher tensile strength, [32–34].

Arboblend V2 Nature typically exhibits a tensile strength of ~40–45 MPa when properly injection molded as a solid part; therefore, the experimentally obtained value of ~10 MPa is more indicative of a defective or weak interface rather than a limitation of the injection-molded material itself, [27, 35]. Overmolding commonly introduces weld/knit lines, residual stresses, and shrinkage or CTE mismatch between the core and the outer layer, all of which can generate interfacial stresses and brittle fracture. These effects are well documented in the overmolding and residual stress literature, [36–38].

– *Processing-induced degradation (particularly of PLA)*: PLA is highly sensitive to moisture; if not dried to below ~0.02–0.025% before processing, hydrolysis occurs in the melt and reduces the molecular weight, leading to a drastic decrease in tensile strength and elongation, and increasing brittleness [39–41]. Elevated temperatures and pressure in the injection barrel accelerate thermal scission, and in the presence of moisture, this effect becomes pronounced, influencing the mechanical performance of the hybrid composite [42].

4.2 Scanning Electron Microscopy (SEM)

Figure 7 shows the microscopic images of the sample in the fracture region (cross-section). A brittle fracture of the composite material is evident, with no observable fibrils, elongated polymer strands, or ductile features in either the biodegradable Arboblend V2 Nature or the PLA component. The detailed view (D) reveals that the printed filaments fractured abruptly, and voids characteristic of the layer-by-layer fabrication process are clearly present within the deposited layers.

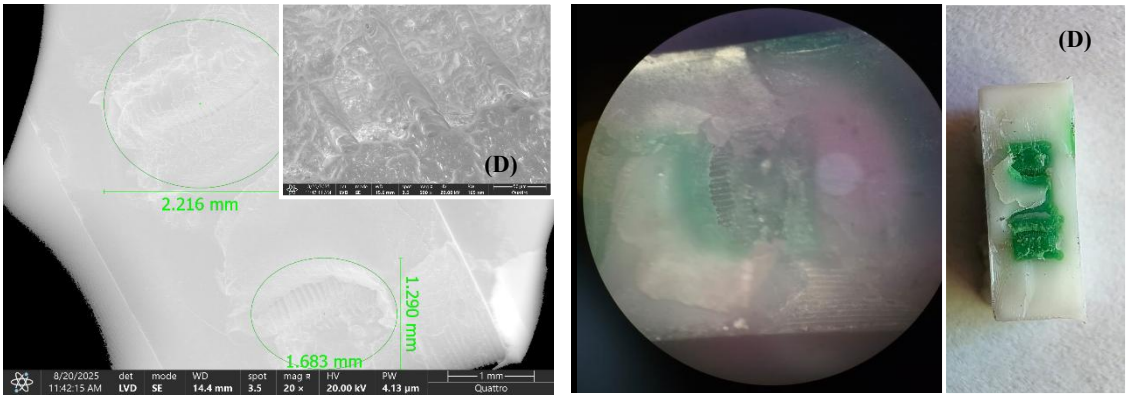

a) SEM image b) Microscopic image

*(D) detail, 500X

Fig. 7. Microscopic images of the sample in the fracture zone

In the longitudinal section of the sample, shown in Figure 8, a significant embedding of the printed support structure (green) within the Arboblend V2 Nature matrix can be observed. All microscopic analyses confirmed this behavior, indicating that the voids designed within the PLA printed support were completely filled by the injected Arboblend V2 Nature. Therefore, the proposed reinforcement support model can be considered suitable for this type of application.

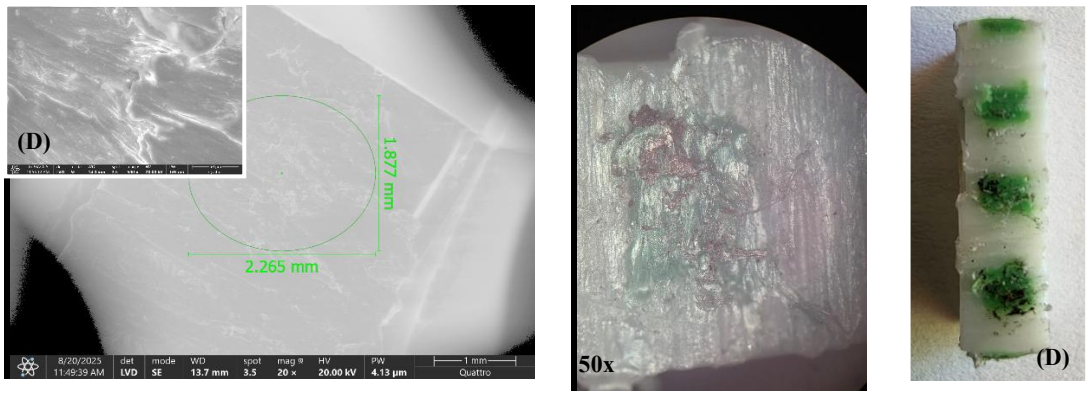

a) SEM image b) Microscopic image

*(D) detail, 500X

Fig. 8. Microscopic images in longitudinal section

5. CONCLUSIONS

Based on the microscopic analysis, the following conclusions were drawn: The surface of the PLA reinforcement structure did not reach a sufficiently high temperature at the moment of contact with the injected Arboblend melt (or may have been contaminated/oxidized), resulting in minimal chain diffusion at the interface. Consequently, interfacial cohesion was weak, even though no cracks, delaminations, or voids were observed. Insufficient drying of the PLA (and/or Arboblend V2 Nature) before processing may have adversely affected the final properties of the part. Residual stresses and differences in shrinkage between the core and the outer shell, combined with weld lines formed in the overmolded layer, may act as stress concentrators and potentially lead to brittle failure.

Therefore, future studies will focus on improving the following aspects: proper drying of the materials used for 3D printing and injection molding; optimization of the printing parameters; preheating the reinforcement structure by heating the active mold plate to enhance adhesion between the printed PLA surface and the injected Arboblend V2 Nature; rounding all corners in the reinforcement model to reduce the likelihood of stress concentrators.

Author Contributions: Conceptualization, S.N.M.; methodology and investigation, S.N.M., D.N.; validation, D.N.; writing - original draft preparation, S.N.M; writing - review and editing, S.N.M.; All authors have read and agreed to the published version of the manuscript.

Funding: This paper has received no external funding.

Conflicts of interest: There is no conflict of interest.

6. REFERENCES

1. Wang Y., Ma H.-S., Yang J.-H., Wang K.-S., (2017), *Industry 4.0: A way from mass customisation to mass personalisation production*, Adv. Manuf., 5(3), 311–320.
2. Bragalia M., Lamastra F.R., Cherubini V., Nanni F., (2020), *3D Printing of polybutadiene rubber cured by photo-induced thiol-ene chemistry: A proof of concept*, eXPRESS Polym. Lett., Vol. 14(No.6), pp. 576–582.
3. Keresztes Z., Pammer D., Szabo P.J., (2019), *EBSD examination of argon ion bombarded Ti-5Al-4V samples produced with DMLS technology*, Period. Polytech. Mech. Eng., 63(3), 195–200.
4. Zhang J., Lu G., You Z., (2020), *Large deformation and energy absorption of additively manufactured auxetic materials and structures: A review*, Compos. Part B Eng., 201(1), pp. 108340.
5. Kotz F., Mader M., Dellen N., Risch P., Kick A., Helmer D., Rapp B.E., (2020), *Fused deposition modeling of microfluidic chips in polymethylmethacrylate*, Micromachines, 11(10), pp. 873.
6. Gutowski T., Jiang S., Cooper D., Corman G., Hausmann M., Manson J.A., Schudeleit T., Wegener K., Sabelle M., Ramos-Grez J., et al., (2017), *Note on the rate and energy efficiency limits for additive manufacturing*, J. Ind. Ecol., 21(1), 69–79.
7. *The New Lightweights: Injection Molded 'Hybrid' Composites Spur Auto Innovation*, Available from: https://www.ptonline.com/articles/the-new-lightweights-injection-molded-hybrid-composites-spur-automotive-innovation, Accessed: 21/01/2025.
8. *CAMISMA's Car Seat Back: Hybrid Composite for High Volume*, Available from: https://www.compositesworld.com/articles/camismas-car-seat-back-hybrid-composite-for-high-volume, Accessed: 21/01/2025.
9. Boros R., Rajamani P.K., Kovács J.G., (2019), *Combination of 3D printing and injection molding: Overmolding and overprinting*, eXPRESS Polym. Lett., 13(10), 889–897.
10. *Overmolded Hybrid Parts Open New Composites Markets*, Composite World, (2019), Available from: https://www.compositesworld.com/articles/overmolded-hybrid-parts-open-new-composites-markets, Accessed: 14/02/2025.
11. Quinlan H.E., Hasan T., Jaddou J., Hart A.J., (2017), *Industrial and consumer uses of additive manufacturing: A discussion of capabilities, trajectories, and challenges*, J. Ind. Ecol., 21(1), 15–20.
12. Popescu D., Zapciu A., Tarba C., Laptoiu D., (2020), *Fast production of customised three-dimensional-printed hand splints*, Rapid Prototyp. J., 26(1), 134–144.
13. Joo S.-J., Yu M.-H., Kim W.S., Lee J.-W., Kim H.-S., (2020), *Design and manufacture of automotive composite front bumper assemble component…*, Compos. Struct., 236(1), 1–12.
14. Janssen H., Peters T., Brecher C., (2017), *Efficient production of tailored structural thermoplastic composite parts by combining tape placement and 3d printing*, Procedia CIRP, 66(1), 91–95.
15. Mark G.T., (2017), *Embedding 3D Printed Fiber Reinforcement in Molded Articles*, U.S. Patent US20170120519A1.
16. Quan Z., Larimore Z., Wu A., Yu J., Qin X., Mirotznik M., Suhr J., Byun J.-H., Oh Y., Chou T.-W., (2016), *Microstructural design and additive manufacturing of 3D orthogonal short carbon fiber/ABS composite*, Compos. Sci. Technol., 126(1), 139–148.
17. Kazmer D.O., Colon A., (2020), *Injection printing: Additive molding via shell material extrusion and filling*, Addit. Manuf., 36(1), pp. 101469.
18. King D., Tansey T., (2003), *Rapid tooling: Selective laser sintering injection tooling*, J. Mater. Process. Technol., 132(1–3), 42–48.
19. Bagalkot A., Pons D., Clucas D., Symons D., (2019), *A methodology for setting the injection moulding process parameters for polymer rapid tooling inserts*, Rapid Prototyp. J., 25(6), 1493–1505.
20. Candal M.V., Gordillo A., Perez O.S., Sanchez J.J., (2008), *Study of the adhesion strength on overmolded plastic materials using the EWIF concept*, J. Mater. Sci., 43(14), 5052–5060.
21. Macedo S., Lafrance E., Martins C.I., Douchain C., Loux C., Krawczak P., (2016), *Thin wall injection-overmolding of polyamide 6/polypropylene multilayer parts*, Int. J. Mater. Prod. Technol., 52(1–2), 53–75.
22. Coogan T.J., Kazmer D.O., (2020), *Prediction of interlayer strength in material extrusion additive manufacturing*, Addit. Manuf., 35(1), 1–12.
23. Han P., Tofangchi A., Zhang S., Desphande A., Hsu K., (2020), *Effect of in-process laser interface heating on strength isotropy of extrusion-based manufactured PEEK*, Procedia Manuf., 48(1), 737–742.
24. Rossing L., Scharff R.B.N., Chömpff B., Wang C.C.L., Doubrovski E.L., (2020), *Bonding between silicones and thermoplastics using 3D printed mechanical interlocking*, Mater. Des., 186(1), 108254.
25. Ma R., Belter J.T., Dollar A.M., (2015), *Hybrid deposition manufacturing: Design strategies for multimaterial mechanisms*, J. Mech. Robot., 7(1), 1–10.

26. Song P., Fu Z., Liu L., Fu C.-W., (2015), *Printing 3D objects with interlocking parts*, Comput. Aided Geom. Des., 35–36(1), 137–148.
27. Nedelcu D., Comăneci R.I., (2014), *Microstructure, mechanical properties and technology of samples obtained by injection from arboblend V2 nature*, Indian J. Eng. Mater. Sci., 21(3), 272–276.
28. Nedelcu D., Mazurchevici S.N., Popa R.I., Lohan N.M., Maldonado-Cortés D., Carausu C., (2020), *Tribological and dynamical mechanical behavior of prototyped PLA-based polymers*, Materials, 13(16), pp. 3615.
29. Cojocaru V., Frunzaverde D., Miclosina C.O., Marginean G., (2022), *The influence of process parameters on mechanical properties of PLA specimens produced by FFF – A review*, Polymers, 14(5), pp. 886.
30. Gajjar T., Yang R., Ye L., et al., (2025), *Effects of key process parameters on tensile properties and interlayer bonding of 3D printed PLA*, Prog. Addit. Manuf., 10(1), 1261–1280.
31. Wang X., Zhao L., Fuh J.Y.H., Lee H.P., (2019), *Effect of porosity on mechanical properties of 3D printed polymers*, Polymers, 11(7), pp. 1154.
32. Akkerman R., Bouwman M., Wijskamp S., (2020), *Analysis of the thermoplastic composite overmolding process: Interface strength*, Front. Mater., 7(1), 1–12.
33. Aliyeva N., Sas H.S., Okan B.S., (2021), *Recent developments on overmolding of thermoset and thermoplastic composites*, Compos. Part A, 149(1), 106525.
34. Giusti R., Lucchetta G., (2020), *Modeling the adhesion bonding strength in injection overmolding of polypropylene parts*, Polymers, 12(9), pp. 2063.
35. Mazurchevici S.N., Mazurchevici A.D., Nedelcu D., (2020), *Dynamical mechanical and thermal analyses of biodegradable raw materials for additive manufacturing*, Materials, 13(8), pp. 1819.
36. Penumetsa V.V., (2021), *Effects of Overmolding Process Parameters on Bondzone Quality*, Doctoral Thesis, Available from: https://scholarcommons.sc.edu/etd/6439, Accessed: 01/02/2025.
37. Kamal M., Lai-Fook R., Hernandez-Aguilar J., (2002), *Residual thermal stresses in injection moldings of thermoplastics*, Polym. Eng. Sci., 42(5), 1098–1114.
38. Parlevliet P.P., Bersee H.E.N., Beukers A., (2007), *Residual stresses in thermoplastic composites – Effects of thermal stresses*, Compos. Part A, 38(6), 1581–1596.
39. NatureWorks LLC, *PLA Processing Guide*, Available from: https://www.natureworksllc.com/~/media/Technical_Resources/Processing_Guides/ProcessingGuide_Crystallizing-and-Drying_pdf, Accessed: 05/01/2025.
40. RTP Company, *PLA Compounds – Molding Guidelines*, Available from: https://www.rtpcompany.com/technical-info/molding-guidelines/pla-compounds, Accessed: 10/01/2025.
41. Velghe I., Buffel B., Vandeginste V., Thielemans W., Desplentere F., (2023), *Review on the degradation of PLA during melt processing*, Polymers, 15(9), pp. 2047.
42. Cuadri A.A., Martín-Alfonso J.E., (2018), *Thermal, thermo-oxidative and thermomechanical degradation of PLA: A comparative study*, Polym. Degrad. Stab., 150(1), 37–45.

Received: September 16th, 2025 / Received in the revised form: November 14 th, 2025 / Accepted: December 15th, 2025 / Paper available online: December 20th, 2025 © International Journal of Manufacturing Economics and Management.